Computational Study of Reynolds Number Effect on Owl-like Wing Aerodynamics at Low Reynolds Numbers

*K. Kondo[1], H. Aono[2], T. Nonomura[2], A. Oyama[2], K. Fujii[2], M. Yamamoto[1]

[1] Department of Mechanical Engineering, Tokyo University of Science, 6-3-1, Niijuku, Katsushika-ku, Tokyo, Japan.
[2] Institute of Space and Astronautical Science/JAXA, 3-1-1, Yoshinodai, Chuo-ku, Sagamihara, Kanagawa, Japan.

*Corresponding author: kondo@flab.isas.jaxa.jp

Abstract

Present study highlights the effects of Reynolds number on aerodynamic characteristics and flow-fields around a rigid stationary cross-sectional owl wing (owl-like wing model) at the Reynolds numbers of 10,000, 23,000 and 46,000. In these Reynolds number regime, the flow-field includes laminar separation, laminar-to-turbulent transition, and reattachment. Therefore, this work employs three-dimensional implicit large-eddy simulation approach that is capable of accurate capturing three-dimensional breakdown of coherent vortices and reattachment physics. Results show that maximum lift-to-drag ratios gently increase comparing with conventional smooth airfoils, while variation of lift-to-drag ratio against the angle of attack appears with increasing Reynolds number. Furthermore, the locations of separation, laminar-to-turbulent transition, and reattachment points on the upper side move to the leading edge side with increasing Reynolds number. These movements have impact on steady and unsteady aerodynamics.

Keywords: Low Reynolds number flow, Aerodynamics, Reynolds number effect, Large eddy simulations.

Introduction

Development of Unmanned Air Vehicles (UAVs) has been an active research area. From the requirement of size, flight speed, and so forth, flight Reynolds number of the UAV becomes the order of 10^4-10^5. Under such low Reynolds number conditions, laminar separation, laminar-to-turbulent transition, sometimes reattachment, subsequently laminar separation bubble is generated so that aerodynamic performance of smooth airfoils, which are generally utilized under high Reynolds number conditions, drastically degrade as shown in Figure 1 (Lissaman, 1983). The behavior of such laminar separation bubble has been investigated by various researchers; the laminar separation bubble affects stalling behavior (Mueller and Batill, 1980) and the response of C_L-α curve (Okamoto, 2005). Therefore, it is important to understand the aerodynamic characteristics associated with the fixed-wing and to study design for high aerodynamic performance UAV wing under such low Reynolds number conditions.

Several researchers have been investigated how to design the airfoil shape in low Reynolds number, and recommended following features (Schmitz, 1980; Laitone, 2005); thin airfoil is better than thick one: the airfoil with camber is better than symmetric airfoil: the sharp leading edge and flat upper surface can improve the aerodynamic ability. Then, we have been interested in the aerodynamic characteristics associated with the avian wings, especially, an owl wing which consists of aforementioned several geometrical features. Additionally, Owl approaches its prey at a moderate speed of 2.5 m/s to 7.0 m/s (Bachmann et al., 2012), so that flight Reynolds numbers based on a mean chord length of approximately 150 mm becomes 25,000 to 70,000. These Reynolds number regimes correspond to UAV flight conditions. Liu et al. (2006) have experimentally measured the owl wing shape and provided mathematical formulation of its shape.

In our previous study, fundamental aerodynamic characteristics and flow-fields around the cross-sectional owl wing based on the experiment data of Liu et al. (2006) are investigated at the

Reynolds number of 23,000 using three-dimensional large-eddy simulations (Kondo et al., 2013). This study focuses on effects of the angle of attack on aerodynamic characteristics and flow-fields at fixed Reynolds number. The results show that the owl-like wing model possesses higher aerodynamic performance than conventional smooth airfoils as plotted in Figure 1. However, it is important to understand the effects of Reynolds number on aerodynamic characteristics of an airfoil when a wing of UAV is designed. Then, present study focuses on effects of Reynolds number on the aerodynamic characteristics and flow-fields around the owl-like wing model. Current work is continuous of the previous study associated with the owl-like wing aerodynamics.
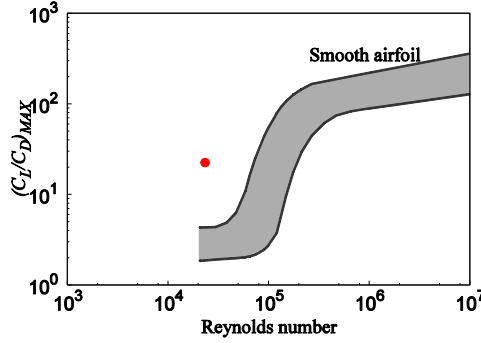

Figure 1. The diagram of Reynolds number effect on maximum C_L/C_D (Lissaman, 1983).

Computational Set-up

Flow Conditions and Model Description

Present study performs numerical simulations for an owl-like wing model at chord-based Reynolds numbers (Re_c) of 10,000, 23,000, and 46,000, a Mach number of 0.2, and the angles of attack (α) of 0.0°, 1.5°, 3.0°, 4.5°, 6.0°, 7.5°, and 9.0°.

The owl-like wing model is the rigid, stationary, and cross-sectional owl wing at 40% span length as shown in Figure 2. This airfoil geometry is constructed based on experiment data by Liu et al. (2006). The owl-like airfoil has a maximum thickness and camber of 5.4% at x/c=0.11 and 4.9% at x/c=0.47, respectively.

Three dimensional implicit large-eddy simulations (3D-iLES) are carried out at the all angles of attack for Reynolds numbers of 23,000 and 46,000. For the Reynolds number of 10,000 where the flow is basically laminar flow regime, two-dimensional laminar simulations (2D-Laminar) are carried out at the all angles of attack as well as 3D-iLES are also performed at selected angles of attack (e.g. 3.0°, 6.0° and 9.0°).
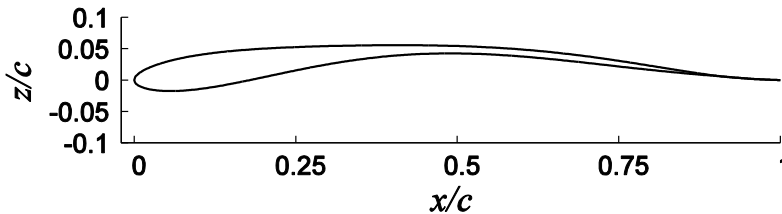

Figure 2. The owl-like wing model.

Computational Methods

Present computations utilize a flow solver LANS3D developed in ISAS/JAXA (Fujii and Obayashi, 1989). The LANS3D solves the compressible Navier-Stokes equations that are normalized by a chord length (c) and the sound speed at a free-stream and generalized in curvilinear coordinates. The spatial derivatives of convective and viscous terms, metrics, and Jacobians are evaluated by the sixth-order compact difference scheme (Lele, 1992) with tenth-order filtering, α_f=0.495, (Gaitonde and Visbal, 2000) for the numerical stability. For time-integration, the second-order backward

difference scheme is converged by the alternating directional symmetric Gauss-Seidel implicit method (Nishida and Nonomura, 2009) with five sub-iterations (Chakravarthy, 1984) in each time step. All computations are performed with a non-dimensional time step of dt=0.00025 so that maximum Courant-Friedrichs-Lewy number becomes approximately 1.9. For turbulent modeling, implicit Large-Eddy Simulation (Boris et al., 1992) approach is adopted. In an iLES, unlike the traditional LES approach, no additional subgrid-scale terms are appended to the governing Navier-Stokes equations. Instead, a high-order low-pass filter selectively damping only the poorly resolved high-frequency waves are employed.

Computational Mesh and Boundary Conditions

Computational mesh around the owl-like wing model is illustrated in Figure 3. C-type structure mesh is utilized for the computational mesh. Grid coordinates are oriented such that ξ traverses clockwise around the airfoil, η follows spanwise direction, and ζ is normal to the surface. Computational mesh consists of 615×201×101 points in ξ, η, and ζ directions, respectively, which is approximately 12 million grid points in total. The first grid points away from the airfoil surface are fixed for all grids and set to be $0.03c/\sqrt{Re}$. The farfield boundary is positioned 30c away from the airfoil in order to reduce its influence on the solution near the airfoil. For the spanwise direction, 20% chord length are computed

At the outflow boundary, all variables are extrapolated from one point inside of the outflow boundary. On the airfoil surface, no-slip adiabatic wall boundary condition is adopted. For the spanwise, 20% chord length are computed with periodic boundary condition to simulate an infinite wing. This boundary condition is imposed using ten points overlap.

Figure 4 shows the grid spacings are evaluated by the wall unit for the current model at Reynolds number of 46,000 and angle of attack of 6.0°. Computational grid in terms of the wall unit satisfies the following inequality in range of turbulence flow region; $\Delta\xi^+ < 25$, $\Delta\eta^+ < 15$, $\Delta\zeta_{min}^+ < 1$ where, $\Delta\xi$ is the clockwise around airfoil, $\Delta\eta$ is the spanwise direction, and $\Delta\zeta$ is normal to the surface minimum grid spacing, and superscript plus donates the normalized value based on the wall unit. With these criteria, the turbulent analysis including near wall flow structure is sufficiently resolved for the present computations. It should be noted that the number of grid points and grid distribution used in current study are determined by grid sensitive analysis. Moreover, grid generation tools and LANS3D have been tested and validated through in a series of previous studies with regard to low Reynolds number flow simulations.
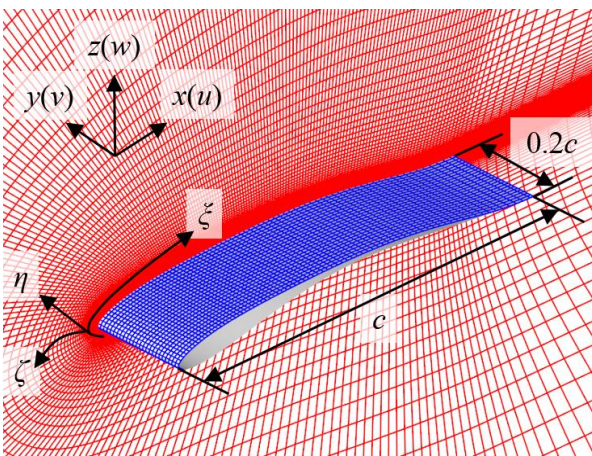

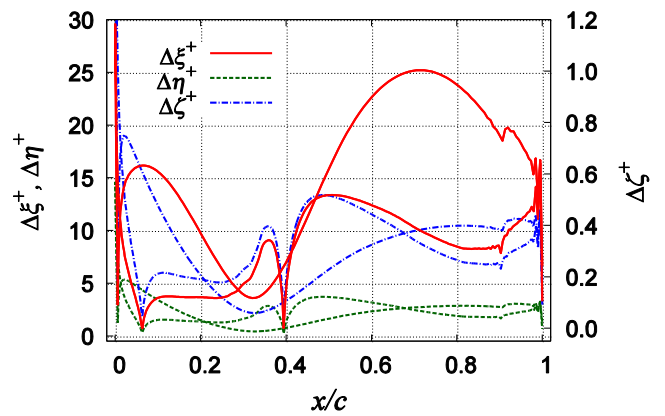**Figure 3. Computational mesh. Grid resolution of 615×201×101.**

Figure 4. Grid-size distribution in the chord direction at *Re*=46,000 and *α*=6.0°.

Results and discussion

Present study highlights the Reynolds number effects of aerodynamic characteristics and flow-fields around the owl-like wing model. To this end, time-averaged aerodynamic force coefficients which are lift and drag coefficients and lift-to-drag ratio are discussed. In addition, surface pressure and skin friction coefficient, locations of separation and reattachment points, time-averaged flow-fields, Reynolds stress, instantaneous flow-fields and time history of the lift coefficients are compared at selected angles of attack of 6.0° to discuss the effects of Reynolds number on flow-fields. The reason that the angle of attack of 6.0° is selected for comparison is that the owl-like wing model attains maximum lift-to-drag ratio at the angle of attack of 6.0° for the Reynolds number of 23,000, and our group has investigated the aerodynamic characteristics at the Reynolds number of 23,000 in previous studies (Kondo, 2013).

Effects of Reynolds Number on Aerodynamic Coefficients

Time-and span-averaged lift-to-drag ratios as a function of the angle of attack and maximum lift-to-drag ratios as a function of the Reynolds number are plotted in Figures 5 and 6, respectively. In addition, time- and span-averaged lift and drag coefficients are given in Figure 7. Before starting discussion of Reynolds number effects, it can be seen that there are differences between the results of 2D-Laminar simulations and 3D-iLES at the Reynolds number of 10,000 and higher angles of attack. It is difficult to estimate the locations of the reattachment points due to limited predictability of laminar-to-turbulent transition by 2D-Laminar.

As the Reynolds number increases, the lift-to-drag ratios increase for all the angles of attack. Moreover, variation of the lift-to-drag ratios against the angle of attack is also large with increasing the angle of attack. Especially, remarkable increment of the lift-to-drag ratio can be seen at the Reynolds number of 46,000 and the angle of attack from 1.5° to 3.0°. Maximum lift-to-drag ratios at the Reynolds number of 10,000, 23,000, and 46,000 are approximately 12 at the angle of attack of 4.5°, 23 at 6.0°, and 33 at 3.0°, respectively. These maximum lift-to-drag ratios of the owl-like wing model are higher than those of smooth airfoils and almost same value with rough airfoils as shown in Figure 6. This figure displays that the owl-like wing model possesses high aerodynamic performance under the low Reynolds number conditions in spite of the smooth airfoil.

Lift coefficients gently increase for almost all of the angle of attack with increasing Reynolds number. Most notably, nonlinearity of lift curves appears at lower angle of attack with increasing Reynolds number. Generally, nonlinearity of the lift curve is related to generation of the laminar separation bubble (Okamoto, 2005). Therefore, it is considered that formation of the laminar separation bubble is promoted as the Reynolds number increases.
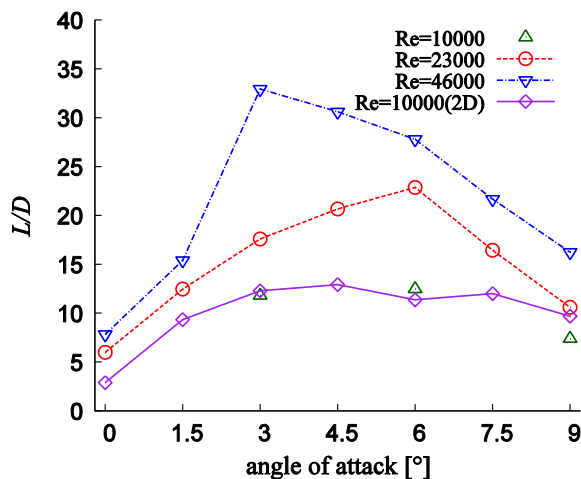

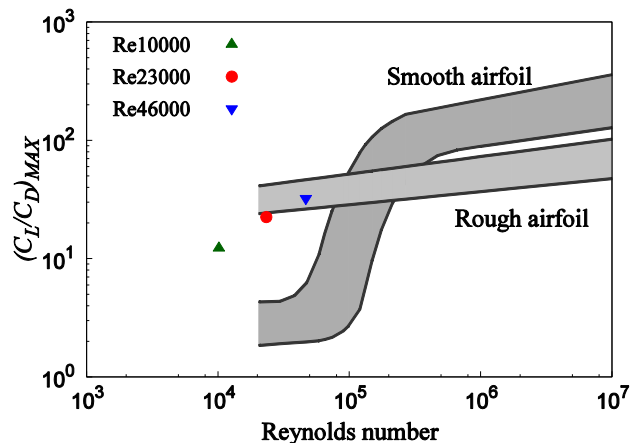**Figure 5. Lift-to-drag ratio as a function of the angle of attack.**

Figure 6. Lift-to-drag ratio as a function of the Reynolds number.
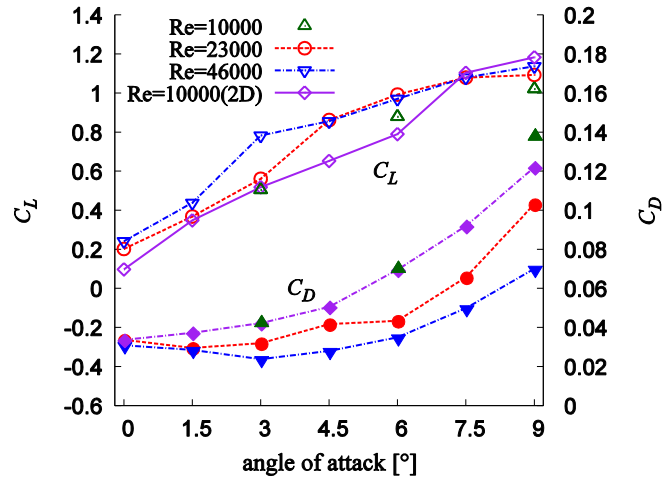
4

Figure 7. Lift and drag coefficients as a function of the angle of attack.

Increasing Reynolds number leads to decrease of drag coefficient for all the angles of attack. Furthermore, it can be seen that there is small variation in the drag coefficient to change of angle of attack. It is interesting that the angle of attack of minimum drag moves toward higher angle of attack with increasing Reynolds number. For instance, the angles of attack of minimum drag at Reynolds number of 10,000, 23,000, and 46,000 correspond to 0.0°, 1.5°, and 3.0°, respectively. This fact implies that flow structure on upper and lower side may or may not have drastic change.

In short, from above discussion, changing the Reynolds number significantly affects the aerodynamic characteristics of the owl-like wing model. The lift coefficient increases, drag coefficient decreases, and, subsequently lift-to-drag ratio is enhanced with increasing Reynolds number. Furthermore, change of the Reynolds number affects nonlinearity of the lift curve and variation of the lift-to-drag ratio against the angle of attack.

Effects of Reynolds Number on Flow Characteristics at Fixed Angle of Attack

Instantaneous iso-surfaces of second invariant of the velocity gradient tensor (*Q*-criterion) with the comparison of time history of the lift coefficients are shown in Figure 8. It is found in all the Reynolds numbers that shear layer separates near the leading edge, develops as going down stream, subsequently generate the dead fluid region in the separated shear layer. Significant differences among three Reynolds numbers are location at which coherent vortices are formed and size of the vortices including three-dimensional vortices structure. Time-history and fluctuation of lift coefficient show influence of location and size of vortices due to change of the Reynolds number.

Time- and span-averaged surface pressure and skin friction coefficients at the angle of attack of 6.0° are given in Figures 9 and 10. There is no difference in the surface pressure coefficients on the lower side for all the Reynolds numbers. On the other hand, the surface pressure coefficients on the upper side display suction peak and relatively flat distribution associated with laminar separation for all the Reynolds numbers. Rapid pressure recovery following the transition and reattachment can be observed except the Reynolds numbers of 10,000. These characteristics of the surface pressure coefficient have been shown in the study of SD7003 airfoil by Uranga et al. (2011). In addition, magnitude of the suction peak and pressure plateau are enhanced, and the location and length of the pressure plateau and pressure recovery move toward the leading edge side as Reynolds number increases. Magnitude of the pressure coefficients near the trailing edge is significantly related to drag generation. As shown in Figure 7, larger drag is generated at the lowest Reynolds number. This is because of difference in the magnitude of pressure coefficient near the trailing edge. There are sudden drops of the skin friction coefficient at certain location of the airfoil in all the Reynolds numbers as shown in Figure 10. This is related to the flow physics such as the separated

5

shear layer rolling up and shedding the coherent vortex from the separated shear layer. The locations of the sudden drop move toward leading edge side with increasing Reynolds number. Furthermore, at Reynolds number of 10,000, downstream of the sudden drop, the skin friction coefficient remains negative. Consequently, it is likely that the flow at the Reynolds number of 10,000 does not reattach unlike the Reynolds numbers of 23,000 and 46,000.

Contours of time-averaged chordwise velocity and Reynolds stress are shown in Figures 11 and 12. Time-averaged flow-fields clearly demonstrate that length of the shear layer becomes shorter and thickness of that also becomes thinner with increasing Reynolds number. In addition increasing Reynolds number leads to reduce the separated region corresponding to blue area in the figures. From these flow-fields, movement of the location of separation and reattachment points to leading edge side is clearly visualized. As shown in Figure 12, small values of Reynolds stress are observed near the trailing edge region for the lowest Reynolds number of 10,000. For Reynolds numbers of 23,000 and 46,000, relatively large values of Reynolds stress are observed near the center of the airfoil. Generally, the location of higher Reynolds stress corresponds to the location where coherent vortex structure that shed from shear layer collapses (see Figure 8). In other words, the increasing magnitude of Reynolds stress is indicative of a more intense laminar-to-turbulent transition process causing the reattachment location. As a result, the locations of reattachment point are located at the just downstream of the highest Reynolds stress for Reynolds number of 23,000 and 46,000.

Effect of Reynolds Number on Separation and Reattachment Characteristics

In previous section, flow characteristics at fixed angle of attack are discussed. It has been clarified that the locations of separation and reattachment point are significantly affected by the change of the Reynolds number. In this section, effects of changing Reynolds number and the angle of attack on separation and reattachment points are discussed.
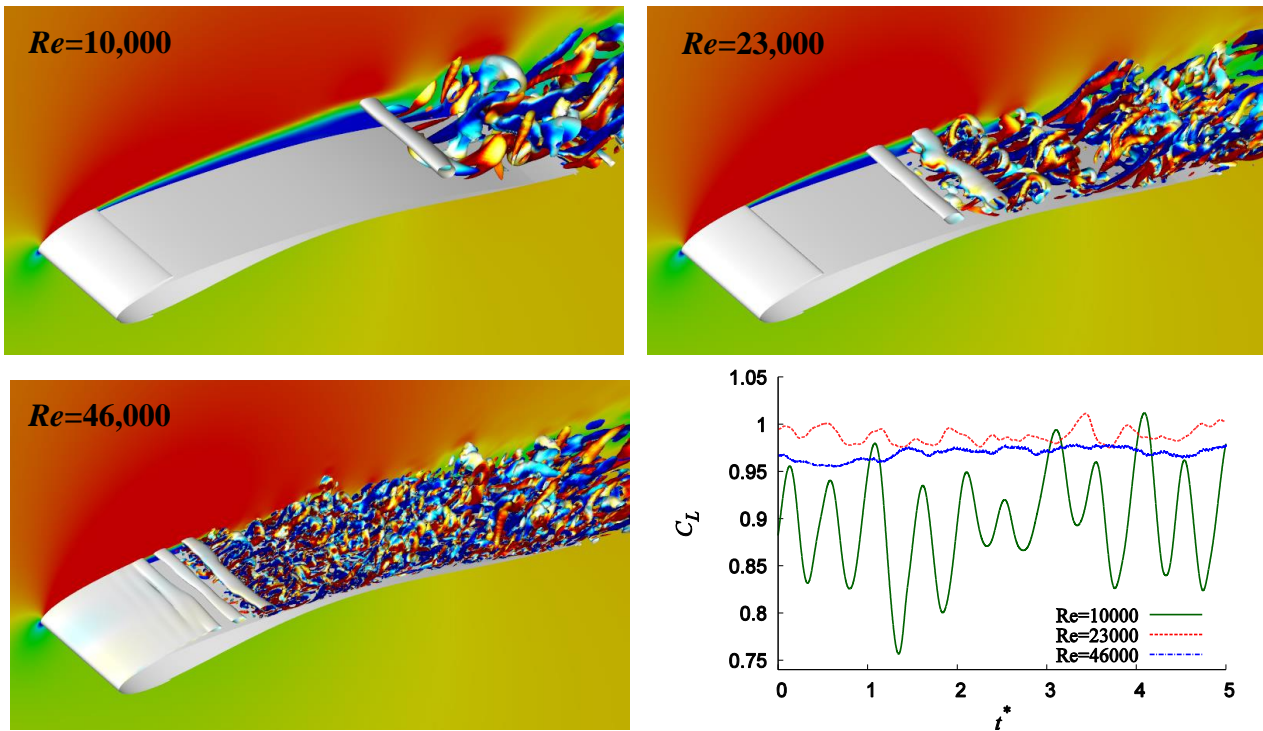

Figure 8. Instantaneous *Q*-criterion (*Q*=5) colored by chordwise vorticity (-5 - 5) with background contours indicating magnitude of chordwise velocity (0 - 1.25), and time history of lift coefficients.
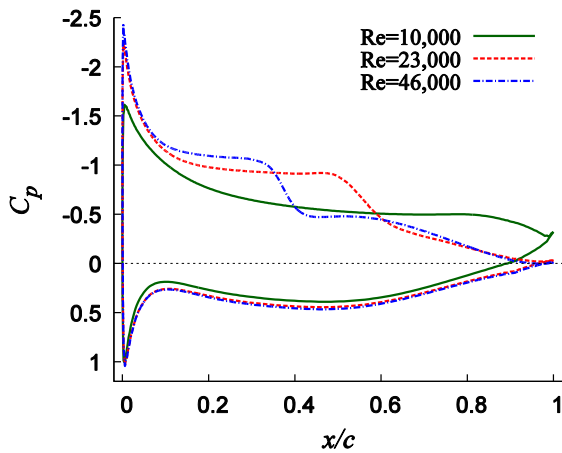
6

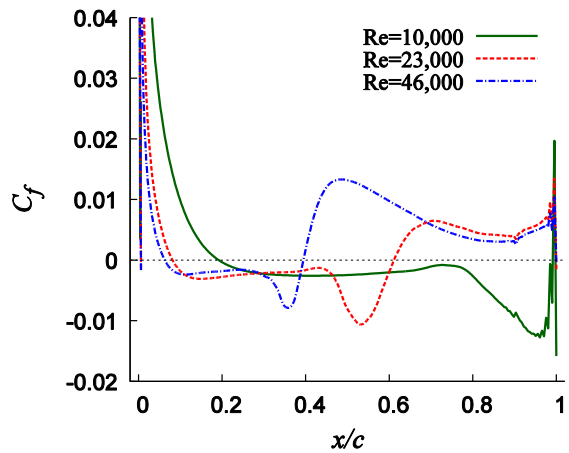**Figure 9. Effects of Reynolds number on surface pressure coefficients for α=6.0°.**

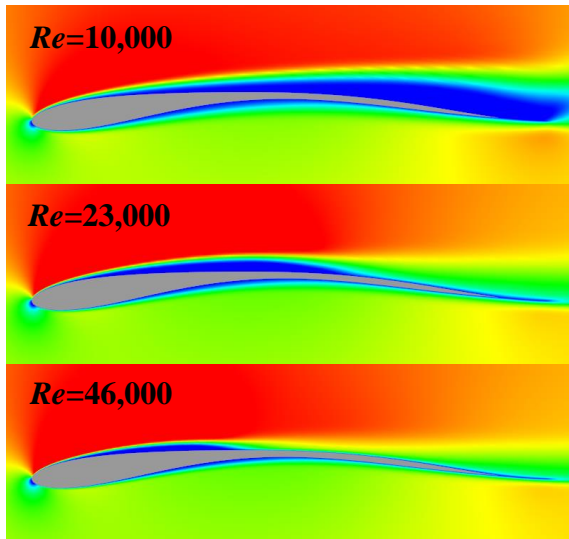**Figure 10. Effects of Reynolds number on skin friction coefficients at α=6.0°.**

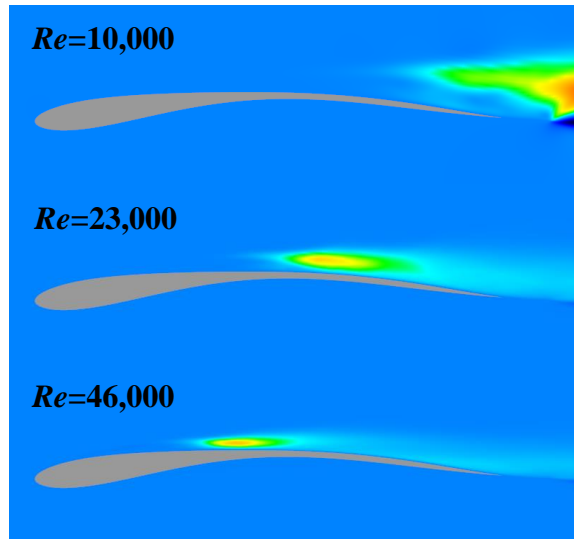**Figure 11. Contours of time-averaged chordwise velocity at α=6.0°.**

Figure 12. Contours of Reynolds stress $(\overline{u'\,w'})$ at α=6.0°.
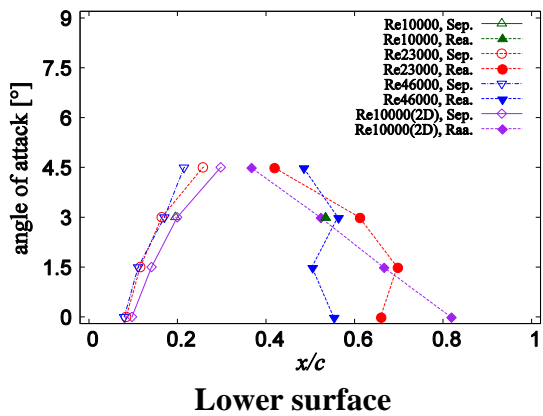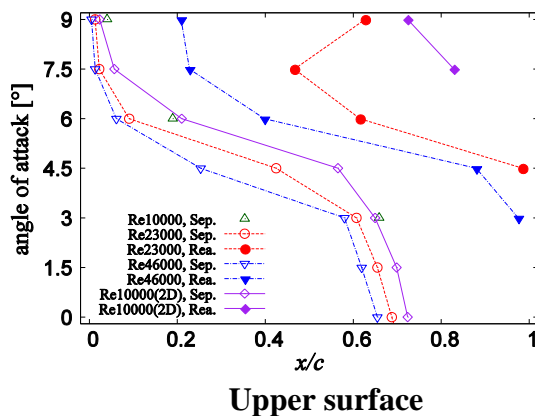

Upper surface

Lower surface

Figure 13. Location of the separation and reattachment points for upper and lower side.

Figure 13 shows the locations of separation and reattachment point as a function of the angle of attack. The locations of separation points on the upper side gently move to leading edge side. A more significant difference in reattachment location is observed among three Reynolds numbers. At Reynolds number of 10,000, the results of 3D-iLES show that the flow does not reattach at all the

7

angles of attack. It is noteworthy that the length of laminar separation bubble between separation and reattachment points becomes shorter and that location moves toward leading edge side with rising Reynolds number. It is noted that the results of 2D-Laminar overestimate in terms of reattachment points at the high angles of attack. This difference between the results of 2D-Laminar and 3D-iLES is currently under investigation. The phenomena of separation and reattachment can be also seen in the lower surface. The locations of the separation points slightly move to the leading edge side with increasing Reynolds number as similar to upper side. However, common features cannot be identified in the behavior of the reattachment points without the angle of attack at which the flow fully attaches. Therefore it is expected that flow-fields on the lower surface are complicated.

Conclusions

Effects of Reynolds number change on the aerodynamic characteristics and the flow-fields around the owl-like wing model are discussed at chord based Reynolds numbers of 10,000, 23,000, and 46,000 and at the angle of attack ranging from 0.0° to 9.0° using three-dimensional implicit large-eddy simulations. Results show that response of maximum lift-to-drag ratio is less sensitive to change of Reynolds number. However, variation of lift-to-drag ratio to change of the angle of attack shows Reynolds number dependency. The locations of separation, laminar-to-turbulent transition, and reattachment point on the upper side move to the leading edge side with increasing the Reynolds number at angle of attack of 6.0°. Noticeable variation of location of separation and reattachment points appears with increasing Reynolds number. Therefore, sensitivity of lift-to-drag ratio to change of the angle of attack is varied due to change of Reynolds number.

Reference

Bachmann, T., Blazek, S., Erlinghagen, T., Baumgartner, W., and Wagner, H. (2012), Barn Owl Flight, Nature-Inspired Fluid Mechanics, volume 119, pp. 101-117.
Boris, J. P., Grinstein, F. F., Oran, E., Kolbe, R. J., (1992), New insights into large eddy simulation, Fluid Dynamics Research, 10, pp. 199-228.
Chakravarthy, S. R. (1984), Relaxation Methods for Unfactored Implicit Upwind Schemes, AIAA Paper 84-0165.
Fujii, K., Obayashi, S. (1989), High-resolution upwind scheme for vertical-flow simulations, Journal of Aircraft, 26(12), pp. 1123-1129.
Gaitonde, D. V., Visbal, R. M. (2000), Pade-type high-order boundary filters for the navier-stokes equations, AIAA Journal, 38, pp. 2103-2112.
Kondo, K., Aono, H., Nonomura, T., Oyama, A., Fujii, K., Yamamoto, M. (2013), Large-Eddy Simulations of Owl-like Wing under Low Reynolds Number Conditions, FEDSM2013-16377.
Laitone, E. V. (2005), Wind tunnel tests of wings at Reynolds numbers below 70,000, Experiments in Fluids.
Lele, S. K. (1992), Compact Finite Difference Scheme with Spectral-Like Resolution, Journal of Computational Physics, Vol.103, pp. 16-42.
Lissaman, P. B. S. (1983), Low-Reynolds-number airfoils. Annual Review of Fluid Mechanics, Vol. 15, pp. 223-239.
Liu, T., Kuykendoll, K., Rhew, R., Jones, S. (2006), Avian Wing Geometry and Kinematics, AIAA Journal, vol.44, No.5.
Mueller, T. J. and Batill, S. M. (1980), Experimental Studies of Separation on a Two Dimensional Airfoil at Low Reynolds Numbers, AIAA Paper, pp. 80-1440.
Nishida, H., Nonomura, T. (2009), Adi-sgs scheme on ideal magnetohydrodynamics, Journal of Computational Physics, 228, pp. 3182-3188.
Okamoto, M. (2005), An experimental study in aerodynamic characteristics of steady and unsteady airfoils at low Reynolds number, Ph.D. thesis, Nihon University.
Schmitz, F. W. (1980), The aerodynamics of small Reynolds numbers, NASA technical memorandum, pp. 51
Uranga, A., Persson, P.-O., Drela, M. and Peraire, J. (2011), Implicit Large Eddy Simulation of transition to turbulence at low Reynolds numbers using a Discontinuous Galerkin method, International Journal for Numerical Methods in Engineering, Vol.87, pp. 232-261.